Detection and Extraction of PFOA and PFOS via MIPs

Joseph Redding

A Senior Thesis submitted in partial fulfillment
of the requirements for graduation
in the Honors Program
Liberty University
Spring 2022

Acceptance of Senior Honors Thesis

This Senior Honors Thesis is accepted in partial
fulfillment of the requirements for graduation from the
Honors Program of Liberty University.

_____
Stephen Hobson, Ph.D.
Thesis Chair

_____
Chad Snyder, Ph.D.
Committee Member

_____
Marilyn Gadomski Peyton, Ph.D.
Honors Assistant Director

_____
Date

Abstract

Perfluorooctanoic acid (PFOA) and perfluorooctane sulfonic acid (PFOS) are utilized as surfactants in many different materials. With an immensely stable structure due to the presence of carbon-fluorine bonds, PFOA and PFOS are resistant to degradation. Known to persist in water resources, these compounds tend to bioaccumulate and impute toxic effects on human health, such as decreased fertility and immune function. To date, there exists no effective approach to the removal of these lingering compounds. Because of the health risks, there is increasing urgency to devise a means by which to detect and withdraw PFOA and PFOS from the environment. In recent years, molecularly imprinted polymers (MIPs) have been proposed as a possible remedy to this threat, due to their unique selectivity and lock-and-key design. This study reviews MIPs as sensors and extractors of PFOA and PFOS. Advancements were made toward the production of a novel fluorinated monomer. A protocol for testing MIPs in aqueous solutions was established and an analysis of a previously made polymer was performed via QCM. The resulting data, though inconclusive, encourages further investigation into the complex fabrication of fluorinated polymers and their analysis via QCM sensors.

Detection and Extraction of PFOA and PFOS via MIPs

PFAS Background

Per- and polyfluoroalkyl substances, or PFAS, are synthetic organic molecules that are found in many different commercial materials. The chemical structure of many PFAS is marked by a charged functional group and an alkyl or ether chain in which many or all hydrogens are replaced with fluorine atoms. The charged functional group and chain length are varied, giving rise to a considerable number of PFAS subtypes. Two PFAS previously used in industry are perfluorooctanoic acid (PFOA) and perfluorooctane sulfonic acid (PFOS). Both PFOA and PFOS possess unique hydrophobic and lipophobic properties that allow them to serve as emulsifiers and surfactants (Teaf et al., 2019). PFOA and PFOS are not naturally occurring substances and were first synthesized in the 1940s as useful chemicals in textiles and other products (Coperchini et al., 2017). Their hydrophobic properties have made them a critical component in water-resistant materials, such as Gore-Tex and nonstick pans (Espartero et al., 2022). In addition, their oleophobic and lipophobic properties have led to their inclusion in paints and fire foams (Coperchini et al., 2017).

The surfactant abilities of PFAS, though suitable in commercial products, are known to contribute to a cytotoxic effect in the human body (Coperchini et al., 2017). The persistence and stability of PFOA and PFOS lead to their bioaccumulation in humans, where they tend to concentrate around the thyroid gland. Naturally, this accretion near the thyroid has been shown to inhibit the circulation of thyroid hormones throughout the body, which may negatively impact the metabolism and immunity of those exposed. This toxic effect is more pronounced in women and children.

Additionally, PFOS and PFOA tend to target organs involved in the immune response, namely the thymus, thyroid, and spleen (Liang et al., 2022). Contact with PFAS has been shown to induce thymus atrophy by way of apoptosis and cytoplasmic reduction. In a study performed on zebrafish, PFOS was demonstrated to induce significant atrophy of the spleen (Zhong et al., 2020). Two other studies using murine hosts corroborated this result, with PFOA and PFOS again causing spleen atrophy (Wang et al., 2011; Wang et al., 2014). Notably, the atrophy of both the thymus and the spleen caused a significant decrease in strength of the subjects' immune response (Liang et al., 2022). It was postulated that the harmful effects of PFOA and PFOS that were observed in the zebrafish and mice would likely translate directly to humans.

Because of its presence in drinking water reserves, PFOA primarily enters the body through oral intake; however, it can also be absorbed through the skin (Liang et al., 2022). One study investigated the relationship between PFOS and PFOA exposure and semen quality and it was discovered that the combined exposure to PFOA and PFOS was directly associated with a lower quality of sperm (Joensen et al., 2009). Another study explored the impact of PFOA and PFOS exposure on fertility in women (Fei et al., 2009). A group of 1,400 randomly selected pregnant women was interviewed and their PFOA and PFOS serum concentrations were tested. An increase in infertility or menstrual cycle irregularity was noted once either PFOS levels reached 26.1 ng/ml or once PFOA levels reached 3.91 ng/ml (Fei et al., 2009). Thus, the study concluded that an increase in PFOA or PFOS exposure is positively correlated with infertility in women.

Recently, studies have also revealed that PFAS hold qualities analogous to carcinogenic agents (Kamendulis et al., 2022; Steenland et al., 2022). The presence of PFAS in the body has been demonstrated to evoke an inflammatory response and induce the generation of reactive

oxygen species. In fact, a study that compared renal cell carcinoma progression with PFOA serum levels in human patients determined PFOA exposure increases the risk of kidney cancer (Steenland et al., 2022). Another study similarly concluded that PFOA contributes to progression of pancreatic cancer (Kamendulis et al., 2022). The mounting evidence of PFA cytotoxicity demands the discovery of a method to detect and remove such chemicals.

Due to the carbon-fluorine bond being one of the strongest known bonds in chemistry, PFAS exhibit remarkable durability and thus resist degradation regardless of the environment (Figure 1; Teaf et al., 2019).

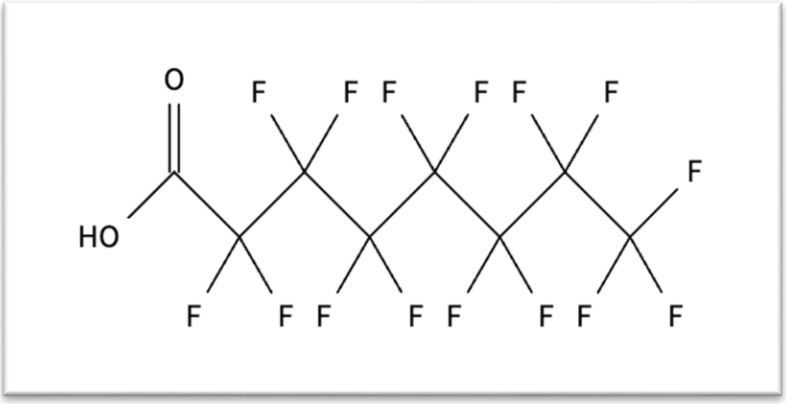

Figure 1. *General Chemical Structure of PFAS (Created by Joseph Redding).*

Note. This figure displays perfluorooctanoic acid (Molecular formula: $C_8HF_{15}O_2$; molecular weight: 414.07 g/mol)

In addition, although they possess a high degree of hydrophobicity, PFAS remain quite soluble in water (Teaf et al., 2019). The water solubility and structural stability of PFAS, combined with their widespread material use, translates to their rampant accumulation in the environment (Wee & Aris, 2023). Despite governmental regulations on their production, PFAS continue to persist in water resources of the United States. The maximum detected concentration of PFOA amounted

to 11,000 ng/L in 2019, which was the highest recorded concentration of a PFAS compound globally (Wee & Aris, 2023). This concerning prevalence is primarily due to PFAS' inherent resistance to all mainstream methods of water purification. Currently, there exists a gap in the literature for the removal of PFAS; however, research has now shifted towards testing molecularly imprinted polymers (MIPs), which have had some success at removing PFOA in the laboratory setting. This study built on the previous success of MIPs and aimed to generate two model compounds that will contribute to future syntheses of MIPs. A protocol for analyzing MIPs was also created and utilized. Before investigating the methods and results, however, the field of MIPs must be understood. To synthesize an MIP that possesses a high selectivity and affinity for these PFAS, it is important to hold a firm comprehension of the science behind molecularly imprinted polymers.

Molecularly Imprinted Polymers

MIPs are an established field in both chemistry and biology because of their ability to bind and remove both small molecules and larger biological molecules. Designed to have a similar binding mechanism to an antibody's binding of a hapten, MIPs appear to be a possible solution to the threat of PFAS (BelBruno, 2019; Zhang et al., 2023). They are highly durable molecules that can withstand a wide range of temperatures, allowing them to be easily stored. Their resilience, in addition to their high affinity, has led them to be applied in many different fields in science, including organic chemistry.

Synthesis of MIPs

The process of designing MIPs begins by selecting the right monomer and can be visualized in Scheme 1 (BelBruno, 2019, p. 95).

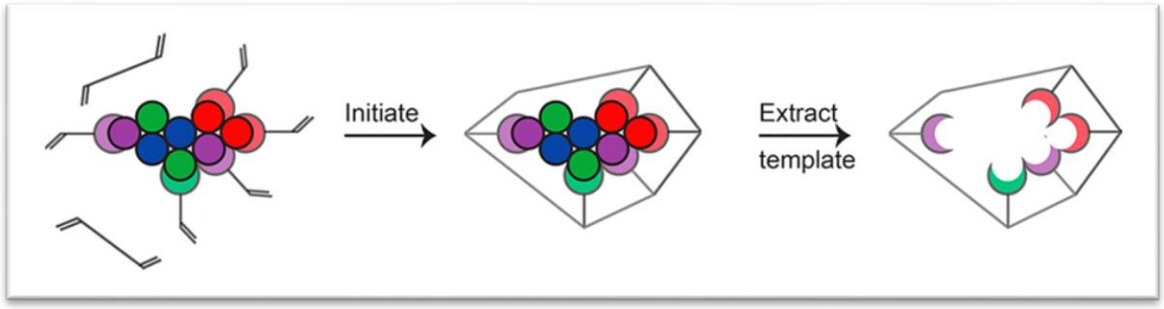

Scheme 1. *Outline of MIP Synthesis.*

One monomer comprising an MIP must be cross-linking and possess functional groups that have a high affinity for the target molecule, or analyte. These monomers will assemble around the analyte (pre-polymerization complex) before a polymerization reaction locks them into formation. Since the analyte will be bound inside the polymer, a binding site is formed with the right size and affinity for the target molecule. The last step in the MIP synthesis is the extraction of the analyte, which leaves an analyte-specific cavity within the MIP. The finished product now possesses high selectivity and affinity for that molecule (BelBruno, 2019).

While the steps described above are ubiquitously followed in MIP synthesis, how the template molecule binds to the cross-linking monomers varies and can be any of three methods: covalent interactions, non-covalent interactions, and semi-covalent interactions.

Covalent Method

The earliest approach to designing MIPs uses covalent bonds to link the monomers with the analyte (Tamayo et al., 2007). Polymerization interlocks these monomers together and the analyte is subsequently removed by breaking the covalent interactions. Now complete, the MIP rebinds its analyte through the rejoining of these covalent bonds. Due to the remarkable strength of covalent bonds, the polymer-analyte connection is highly stable, minimizing the non-specific sites in the binding cavity (BelBruno, 2019). Nevertheless, this bonding strength only permits

analyte separation from the MIP under extreme conditions. Given that the usual application of MIPs demands mild conditions (e.g. living organisms or environmental testing) this aspect of covalent MIPs limits their commercial application.

Non-covalent Method

In 1984, Mosbach and Sellergren engineered another method of designing MIPs, in which they utilized bonds of a weaker binding capacity (Andersson et al., 1984). Instead of employing covalent bonds between the analyte and monomers, this second method uses ionic bonds, hydrogen bonds, or other interactions to link the template molecule with the crosslinking monomers (Tamayo et al., 2007). Because these chemical bonds are weaker than covalent interactions, they grant MIPs the ability to dissociate from the analyte under a variety of conditions; thus, non-covalent MIPs have a wider scope of application. A secondary advantage to this approach is that it involves both experimental procedures and monomer functional groups that are simpler and easier to synthesize than the covalent method. However, one notable downside is that the weaker non-covalent bonds lead to less precise imprinting than that of covalent bonds. The number of non-specific sites generated by non-covalent bonds is a known complication in the design process that has hindered the advancement of MIPs (BelBruno, 2019). In order for an MIP to be effective, it is necessary for there to be a minimal number of non-specific sites in the binding cavity.

Semi-Covalent Method

The third approach for binding the analyte to the monomers combines the aforementioned methods and is termed semi-covalent. In the polymerization step, the analyte and monomer bind using covalent interactions (Lübke et al., 1998). After the analyte has been removed, the polymer rebinds with analyte via non-covalent bonds. This approach has mostly been limited to targeting

analytes that are aromatic, such as polychlorinated aromatic compounds, due to their ability to form weak hydrogen bonds (Effting et al., 2024).

For this study, the non-covalent approach was chosen, due to its high degree of binding reversibility and simplicity of procedural steps (Tamayo et al., 2007). While the synthesis for non-covalent MIPs is a relatively straightforward process, the reaction requires an excess of monomers to overcome the reaction equilibrium. This often leads to non-binding sites that may disrupt the selectivity and efficiency of the MIP.

Applications of MIPs

The extensive literature on MIPs reveals they have many different applications, including water purification, pharmaceutical production, and decontamination of commercial products. A recent review by Zhang et al. (2023) discussed the importance of MIPs in the production of various medications and therapeutic agents in healthcare. For instance, MIPs demonstrated significant durability and high selectivity for quercetin, setting it apart as an extractor of this known flavonoid (Figure 2; Patil & Masand, 2018, p. 402).

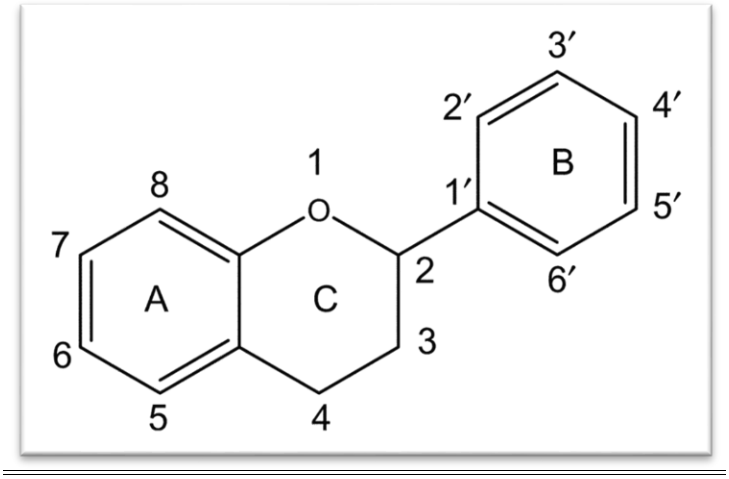

Figure 2. *Basic Structure of Flavonoids.*

Found in plants, flavonoids comprise an extremely important class of substances that are used as a treatment for cancer, inflammation, and cardiovascular disease (Zhang et al., 2023). While they resist most forms of purification, flavonoids have been extracted from plants in high yields via MIPs.

Another function of MIPs is controlled drug release delivery. Their environmental sensitivity allows them to be synthesized in such a way as to release a template drug in a specific bodily location. One author argued that this quality makes MIPs the ideal oral colon-specific drug delivery system (Zheng et al., 2016). MIPs have been shown to delay release of an oral medication until entering the colon, allowing colon-targeting drugs to be released there in high concentrations, increasing their effectiveness while minimizing side effects. Though MIPs are flush with benefits, one drawback to their application is that extractions in water often create competition between the MIPs and water molecules for the analyte (Zhang et al., 2023). Both the MIP and water can attract the analyte with non-covalent bonds–water attracts via hydrogen bonds–and this dampens the affinity of the MIP for the analyte. This downside may complicate liquid extractions of PFOA and PFOS with MIPs.

Despite this potential drawback, there are numerous studies demonstrating MIPs' success in liquid solutions as sensors and extractors of molecules. In a study performed recently, MIPs were employed to selectively remove the toxic chemical arsenic from water (Kirisenage et al., 2022). Arsenic is a toxic ingredient in insecticides that is commonly found in groundwater throughout the world. While several methods already exist for extracting this compound, MIPs are more desired because of their general efficiency, low cost, and selectivity. In the study, MIPs were shown to be highly selective in their adsorption and removal of arsenic (Kirisenage et al.,

2022). The durability of MIPs was also noted, with the MIPs maintaining their integrity regardless of the environment.

Another article demonstrated the effectiveness of MIPs at detecting ractopamine, the potentially toxic feed additive for pigs which is illegally used to promote livestock muscle mass (Pan et al., 2018). In the study, researchers coated a quartz crystal microbalance (QCM) with an MIP specific for ractopamine. The results of this study revealed that the molecularly imprinted piezoelectric sensor was highly accurate, precise, and sensitive in its detection of ractopamine. While the experiment was not conducted in water, it utilized a QCM in the detection of chemicals, which is the analysis platform of choice in this study.

While there remains a gap in the literature regarding fluorinated MIPs in the detection and extraction of aqueous chemicals, a recent study provides encouraging results concerning this specific application of MIPs (Cennamo et al., 2018). This research article demonstrated positive fluorinated MIP binding to PFAS in a liquid solution, an important breakthrough for the field of fluorinated MIPs. In contrast to the traditional analytical methods of PFAS that pair chromatography with mass spectroscopy, the study used a surface plasmon resonance (SPR) instead. This analytical method, which uses plastic optical fibers, poses as a cheaper and easier-to-use option than previous methods. In the study, an MIP was synthesized with a fluorinated backbone, allowing the fluorinated MIP (fMIP) to bind through noncovalent interactions with the PFAS. SPR was used in combination with this novel fMIP to detect the PFAS. The pairing of SPR with fMIPs proved effective, detecting very low concentrations of PFAS in water (0.13 ppb). The MIPs were compared to non-imprinted polymers (NIPs), which served as a control, and the MIPs displayed significantly higher selectivity to the PFAS in the study compared to

NIPs. The various applications of MIPs reveal a unique set of traits, including selectivity and effectiveness in chemical adsorption in water, that make them ideal for the removal of PFAS.

Fluorinated MIP Chemistry

For an MIP to have exceptional sorption of PFAS, it must contain functional groups that maintain strong positive interactions with the fluorine atoms that line the carbon backbone of PFAS. Fluorine atoms will augment the surrounding electrostatic interactions and will serve as the ideal functional group for MIPs. Although fluorine atoms are typically known to have weak negative interactions between themselves, one author argues that the Vander Waals interactions of fluorine atoms may combine to generate cohesive forces between fluorinated molecules (Kong et al., 2022). Another author similarly asserted that hydrophobic fluorine-fluorine interactions are sufficient for the adsorption of PFAS with polymers (Tan et al., 2022). When coupled with the binding between carboxylic acid and an amide functional group, fluorine-fluorine interactions improved binding and sorption of PFAS molecules.

Past Work of Hobson Research Group

This study is a continuation of research conducted previously by the Hobson Research Group. The results of this prior phase culminated in the synthesis of 2 MIPs, an associated non-imprinted polymer (NIP), and the analysis of their performance. To determine their efficacy, 4 MIPs (STH91 and STH153-155) were sent post-synthesis to Seacoast Science for analysis with a QCM and chemiresistor. MIP production was initiated with the synthesis of **1** (Scheme 2).

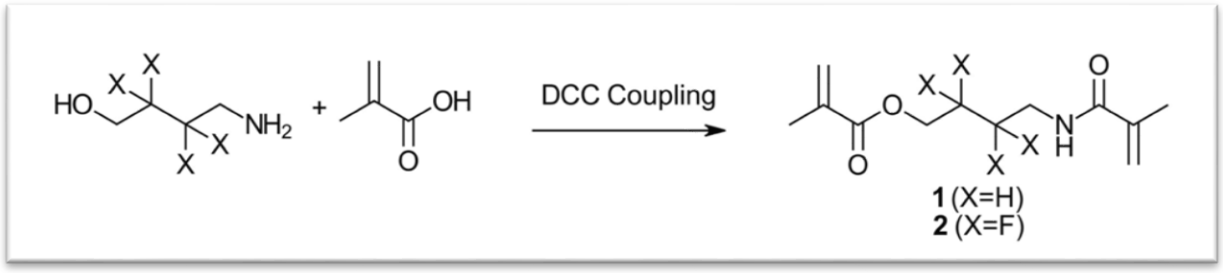

Scheme 2. *Synthesis of Cross-Linking Monomers **1-2.** (Created by Dr. Stephen Hobson)*

Building on the work of Spivak, methacrylic acid and 4-amino-1-butanol were coupled using DCC to form functionalized crosslinking monomer **1** (Sibrian-Vazquez & Spivak, 2004). Isolation of product was achieved by filtration, extraction of organic phase, and a washing step via sodium bicarbonate. *In vacuo* removal of solvent gave way to a yield of 80 percent at a 50 mmol scale. Note that **1** is nonfluorinated, and **2** (perfluorinated) was unable to be synthesized (Scheme 2). Characterization of **1** was achieved by both Fourier-transform infrared spectroscopy (FTIR) and nuclear magnetic resonance (NMR) spectroscopy (Figures 3, 4).

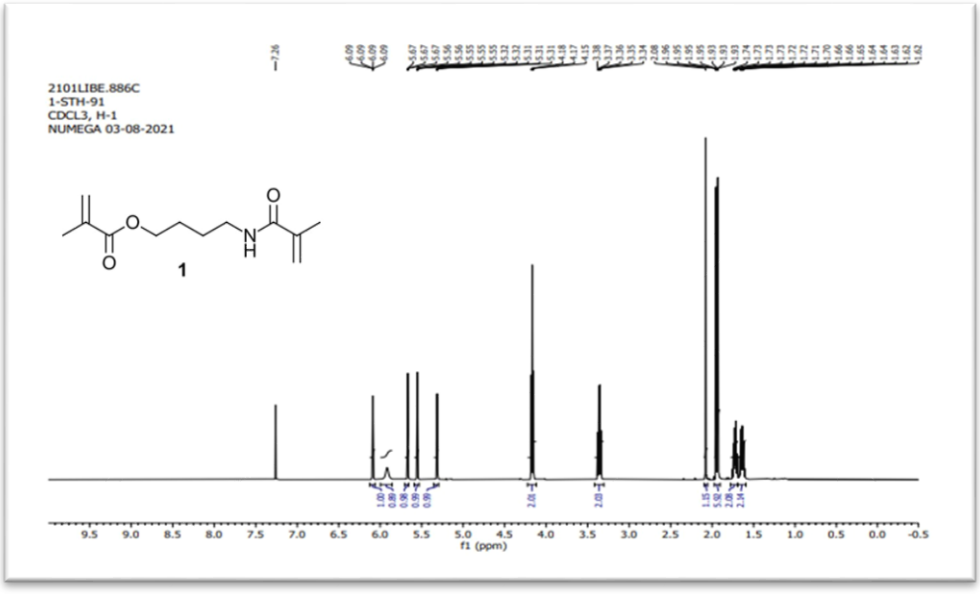

Figure 3. *^{1}H NMR Spectrum of Monomer **1** (Created by Dr. Stephen Hobson).*

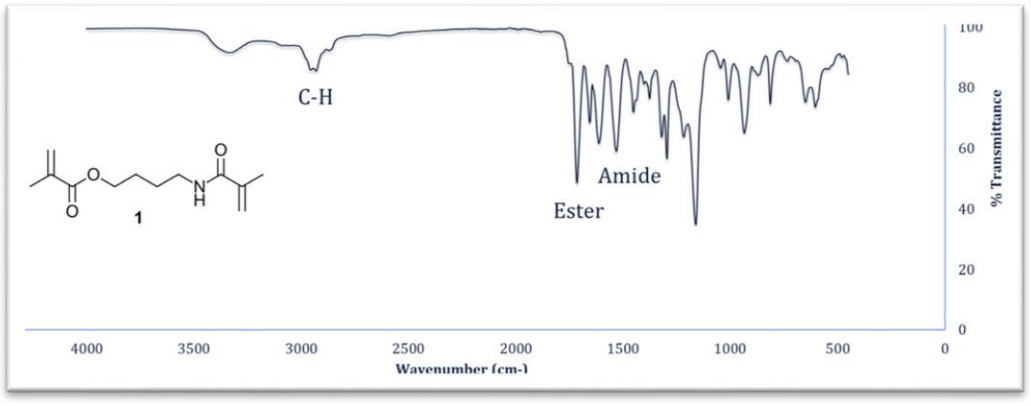

Figure 4. *FTIR of Monomer **1** (Created by Dr. Stephen Hobson).*

Two distinct polymerization reactions were performed using **1** (Scheme 3).

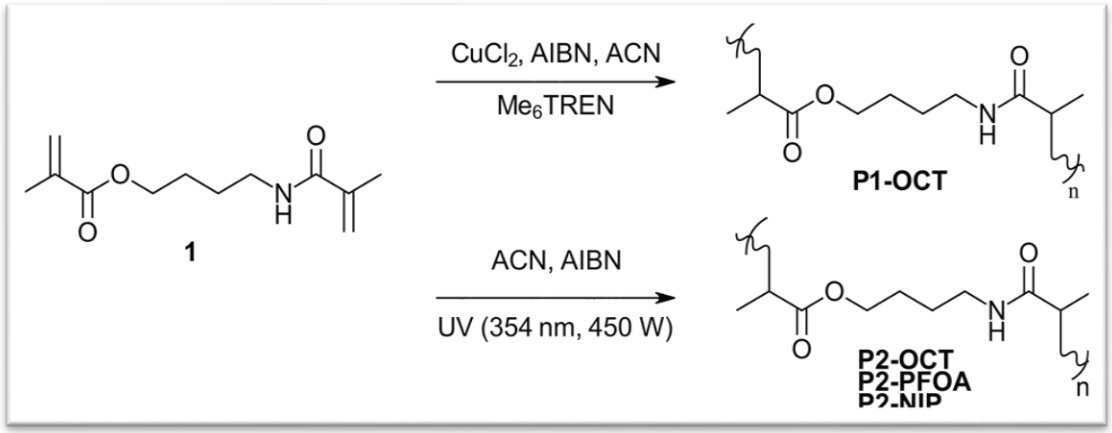

Scheme 3. *Polymerization Conditions for Monomer **1** (Created by Dr. Stephen Hobson)*

Note. P1-OCT is the OA-imprinted MIP (STH91) and P2-OCT, P2-NIP, and P2-PFOA are STH153, STH154, and STH155, respectively.

Reaction P1 involved an atom transfer radical precipitation polymerization as described in a previous study (Zu et al., 2009). A workup via Soxhlet extraction produced moderate yield of an OA-imprinted MIP. However, the success of this reaction was unable to be repeated in subsequent attempts, regardless of the presence of an imprinting molecule. A new approach was attempted, reaction P2, in which the radical polymerization was UV-initiated. With AIBN as the

initiator, **1** then underwent three separate UV-induced polymerizations in the presence of octanoic acid, PFOA, and in the absence of a template molecule, respectively (Scheme 3). Since the structure of **1** lacked fluorine atoms, assembly around the chosen analyte was achieved through exclusively electrostatic and hydrogen bonding interactions. A washing step removed template molecule and possible impurities. Isolation via centrifuge produced a moderate initial yield of MIPs. Overall, the polymerization initiated by UV exposure produced greater product yield and expedited purification compared to reaction P1.

Seacoast Science determined the binding affinity and selectivity of the newly synthesized MIPs by way of QCM and chemiresistor technology. QCMs are piezoelectric sensors that can precisely sense the quantity of any desired target bound to the quartz crystal; a change in the resonance frequency is correlated to a change in the amount of molecule bound to the QCM chip (Pan et al., 2018). For this analysis, the newly synthesized MIPs (STH91 and STH153-155) dispersed into a poly(ethylene-co-vinyl acetate; PEVA) matrix and were deposited onto the surface of their respective quartz crystals via drop casting. A PEVA-coated QCM was created as a control. Each QCM was tested against four separate diluted solutions: octanoic acid, acetic acid, PFOA, and PFOS. Relative binding for each test was calculated by comparing the shift of the resonance frequency in solution to that of deionized water. The normalized response of the coated QCM was then determined by using the Sauerbrey equation (Equation 1), which adjusted for the mass of polymer on the QCM chip (Δm is mass change; Δf is frequency shift; C_{QCM} is mass sensitivity constant; Huang et al., 2017).

$$\Delta m = -C_{QCM} \times \Delta f \qquad \text{(Equation 1)}$$

The responses revealed that PFOA and PFOS were more effectively adsorbed by the three MIPs than the controls in Figure 5 (created by Seacoast Science).

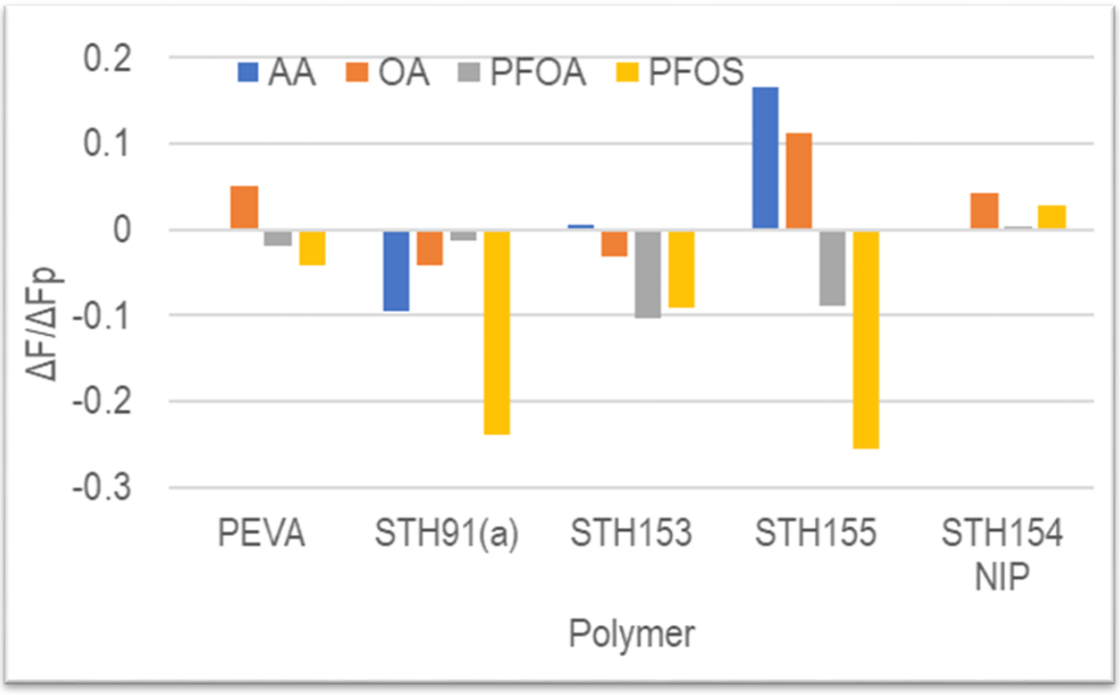

Figure 5. *QCM Data for Binding of PFOA and PFOS.*

Note. Normalized responses of each coated QCM shown relative to mass of polymer coating. ΔFp represents the frequency shift of the polymer and is < 0. (OA and AA are octanoic acid and acetic acid, respectively).

Seacoast verified the acquired QCM data by testing the MIPs with chemiresistor platforms. As opposed to QCM technology, chemiresistive sensors measure analyte binding by sensing changes in the resistance of the polymers (Hua et al., 2022). A chemiresistor platform involves a sensitive material that is deposited across electrodes, creating a modulable resistor. In the presence of an analyte, the electrical resistance of the material changes, allowing the presence or mass of analyte to be determined. A significant resistance modulation from baseline indicates

successful analyte binding. Conducting particles in a resistive polymer matrix (CPs) were the type of sensing material highlighted (Huang et al., 2008). A change in the interparticle distance in the insulating polymer matrix causes a concomitant change in resistance of the matrix. This change in resistance is measured by the chemiresistor platform. One downside to the use of this type of polymer/conductive particle matrix is lack of selectivity; however, integrating MIPs into this system has been shown to negate this problem and increase the analyte sensitivity of CP chemiresistors.

At Seacoast Science, two sets of CP chemiresistors were produced. One set consisted of blending each polymer with conductive carbon, while the other was a 50:50 blend of PEVA/MIP that was subsequently mixed with conductive carbon black. Two types of chemiresistor platforms were employed: ceramic and printed circuit board (PCB). Seacoast determined that the ceramic platform translated to a greater degree of polymer binding than the PCBs, so results from the ceramic set of tests will be shown (Figure 6; created by Seacoast Science).

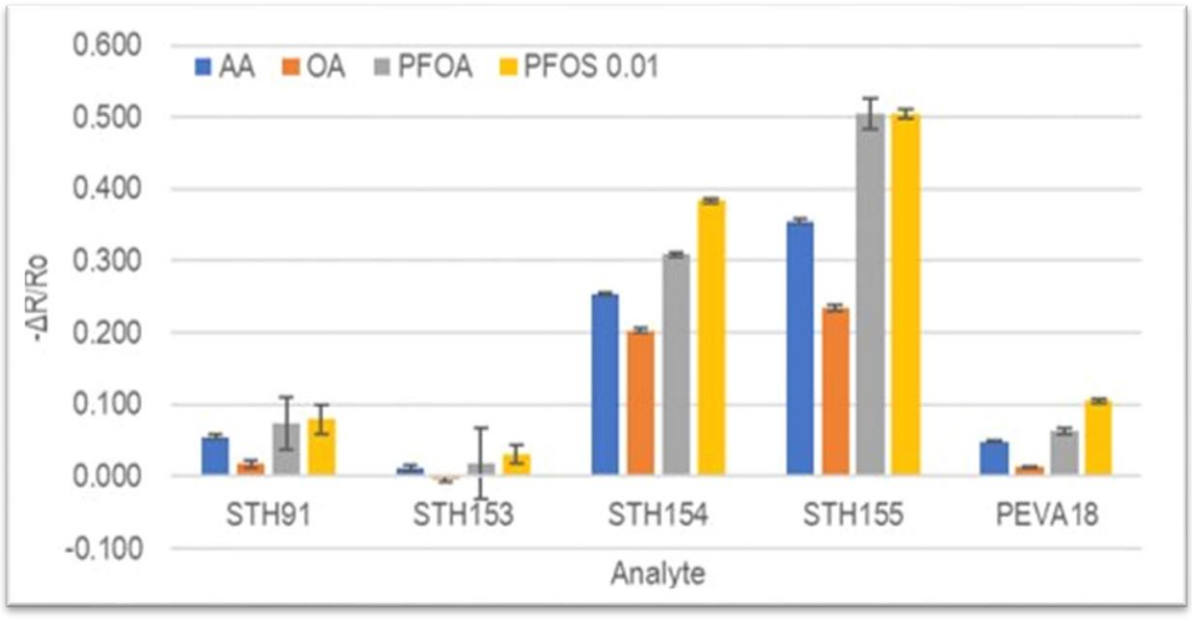

Figure 6. *Chemiresistor Responses of MIPs vs PFAS.*

Note. Each analyte solution had a concentration of 0.01%.

The results of the chemiresistor platform displayed less selectivity by MIPs toward PFOA and PFOS. In addition, STH154 (NIP) had a more similar pattern of binding to STH155 than was found in the QCM results. Although the chemiresistor data conflicted with the QCM data, both platforms revealed that both MIPs had a higher effectiveness than PEVA control. Of note, it was postulated by the Hobson Research Group that at the high solution concentration of 0.01%, the solution conductivity may have complicated the results.

Evidence provided by QCM attests to the selectivity and affinity of the synthesized MIPs toward PFOA and PFOS. Chemiresistor results, though conflicting in regard to sensitivity, verified that the MIPs possess higher affinity to the analytes than do the controls. These findings justified a continuation of this research study.

Current Work of Hobson Research Group

The previous results of Hobson Research Group demonstrated the efficacy of MIPs in the adsorption of PFOA and PFOS in a liquid source. However, there remains a gap in the literature regarding the successful synthesis and application of fluorinated molecularly imprinted polymers (fMIPs) toward the detection and extraction of PFOA and PFOS. Building on the past results of the Hobson Research Group, continued research was performed concerning the synthesis of fMIPs for the purpose of detecting and extracting PFOA and PFOS from water resources. We postulate that the production of an MIP containing fluorine atoms, as compared to the previously synthesized polymers (STH91 and STH153-155), will bind with higher affinity and selectivity due to the presence of the fluorine-fluorine interactions (Tan et al., 2022).

Furthermore, a standard protocol was formulated for efficient analysis of future MIPs. Such protocol was necessary due to cessation of the agreement with Seacoast Science involving

analysis of the fabrications by Hobson Research Group. To verify polymer results acquired previously by Seacoast Science, an analysis of STH153 was also performed by way of a QCM sensor.

Method

Monomer Syntheses

In this study, the syntheses of two model compounds, a fluorinated compound and a nonfluorinated compound, were attempted, and the synthesis steps of the nonfluorinated compound is shown in Scheme 4. Note the final 3+2 cycloaddition step used phenylacetylene as a model compound. Future work will replace phenylacetylene with 2-methylpent-1-en-4-yn-3-one to produce a functionalized crosslinking monomer.

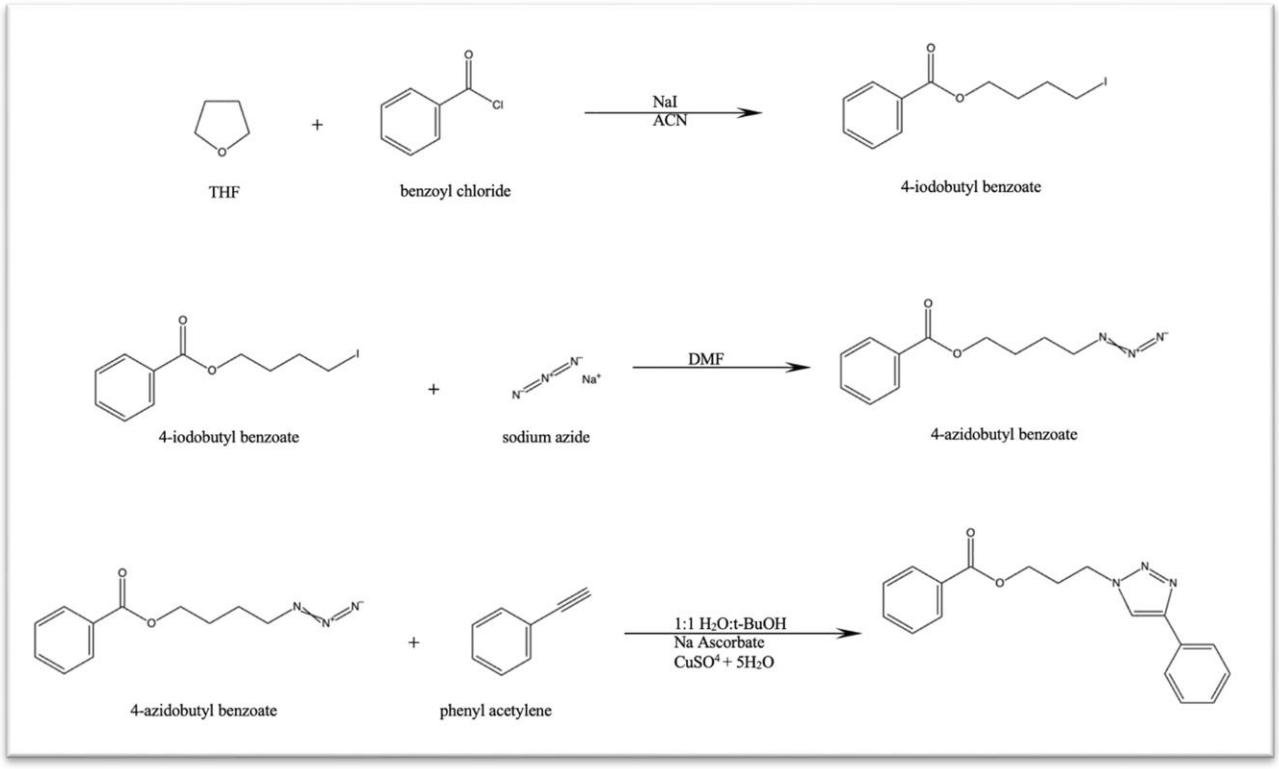

Scheme 4. *Schematic of Model Crosslinking Compound **3.** (Created by Joshua Kim)*

Synthesis of Model Compound 3

4-iodobutyl benzoate (Bates & Dewey, 2009). Benzoyl chloride (1.154 g) was added to a solution of sodium iodide (2.398 g), tetrahydrofuran (1.154 g), and acetonitrile (1 mL; Scheme 4). The reaction was stirred in the absence of light and left to run at room temperature for 72 hours. Solution was diluted with deionized water (20 mL) and diethyl ether (20 mL). Organic phase was isolated and aqueous phase was washed three times with diethyl ether (30 mL). Organic phase was recombined and then washed in a stepwise manner with saturated solutions of sodium bisulfite (5 mL) and sodium carbonate (5 mL). Solution underwent a drying step with magnesium sulfate, filtration, and then solvent removal *in vacuo*, to produce 4-iodobutyl benzoate (2STH170) for a yield of 66 percent (3.221 g).

4-azidobutyl benzoate (Dewey, 2010). Sodium azide (1.040 g) was dissolved in a solution containing 2STH170 (3.221 g) and DMF (15 mL; Scheme 4). In the presence of an ice bath that was left to warm up naturally, reaction ran for 72 hours in the absence of light. Solution was diluted with deionized water (10 mL) and diethyl ether (10 mL). Organic phase was isolated and aqueous phase was washed 3 times with ether (5 mL). Organic phase was recombined and concentrated *in vacuo*. Remaining mixture was resuspended in hexane (10 mL), washed with sodium chloride (3 mL), and dried with magnesium sulfate. Solution was filtered and concentrated *in vacuo*, producing 4-azidobutyl benzoate (2STH176) with a yield of 77.65 percent (1.803 g). Infrared (IR) spectroscopy of product was taken to confirm identity.

***4-(4-phenyl-1H-1,2,3-triazol-1-yl)butyl benzenecarboxylat*e** (Jia et al., 2022). Working solutions of sodium ascorbate (0.9999 M) and copper sulfate (0.3000 M) were made with deionized water as the diluent. Phenyl acetylene (0.36 mL), 4-azidobutyl benzoate (0.721 g), and a 1:1 (v/v) mixture of deionized water and tert-butyl alcohol (13 mL) were added to a reaction flask. From

prepared working solutions, sodium ascorbate (300 µL) and copper sulfate (100 µL) were poured into the reaction mixture (Scheme 4). Reaction was stirred at room temperature for approximately 43 hours. The reaction was extracted 3 times with ethyl acetate (25 mL) and the combined organic phases were washed with deionized water (15 mL), followed by sodium chloride (10 mL). Solution was dried with magnesium sulfate, filtered, and then concentrated *in vacuo*. IR spectroscopy of product was acquired to confirm its identity. Purification of product was performed with column chromatography, using a 1:1 (v/v) mixture of hexane and ethyl acetate as the mobile phase and silica as the stationary phase.

Synthesis of Monomer 4

The synthesis of fluorinated model compound **4** involved a four-step reaction process that began with the synthesis of 2STH184 (Scheme 5).

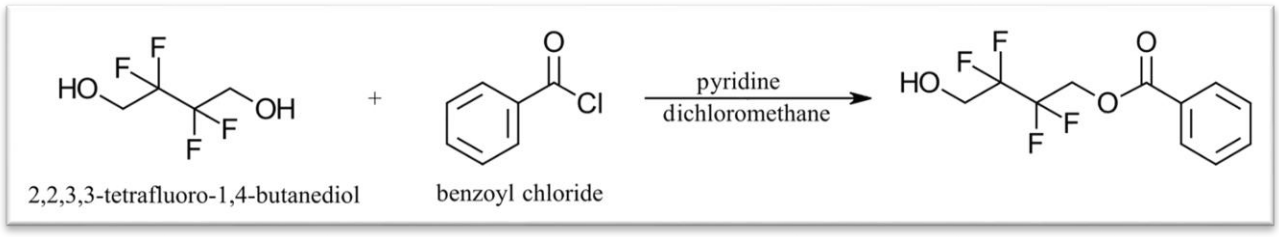

Scheme 5. *Fluorinated Monomer Synthesis. (Created by Joshua Kim)*

2,2,3,3-tetrafluoro-4-hydroxybutyl benzenecarboxylate (Nortcliffe et al., 2014). 2,2,3,3-tetrafluoro-1,4-butanediol (3.33 g) was dissolved in a solution containing benzoyl chloride (3 mL), pyridine (3.2 mL), and dichloromethane (16 mL). After running for 72 hours at room temperature, the reaction was washed 2 times with deionized water (30 mL), 2 times with HCL (50 ml), and 2 times with sodium bicarbonate (50 mL), followed by a drying step with magnesium sulfate. 2STH184 was isolated *in vacuo* for a yield of 67.4 percent (2.62 g).

For the synthesis of 2STH187, a tosylation reaction was employed (Scheme 6).

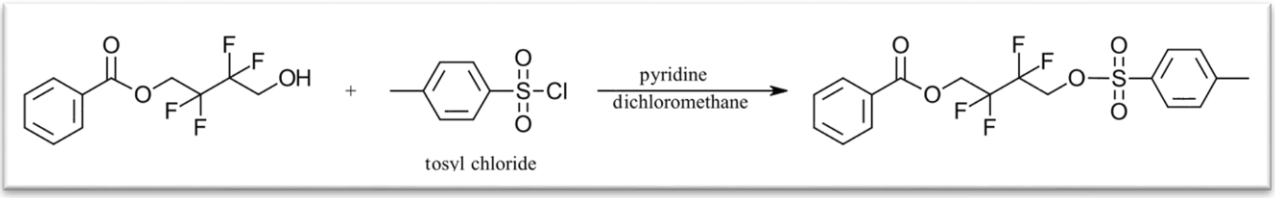

Scheme 6. *Tosylation of fluorinated benzoate. (Created by Joshua Kim)*

2,2,3,3-tetrafluoro-4-(4-methylphenylsulfonyloxy)butyl benzenecarboxylate (Li et al., 2009). 2STH184 (2.62 g) was added to a solution containing tosyl chloride (3.2 g), pyridine (0.89 g), and dichloromethane (22 mL). After running for three days at room temperature, the reaction was concentrated *in vacuo*. Remaining mixture was resuspended in 20 mL of ethanol and then dried with sodium bicarbonate. The mixture was extracted 3 times with ethyl acetate (15 mL), washed with sodium chloride, and dried with magnesium sulfate. Solvent removal *in vacuo* produced 2STH187 for a yield of 84.5 percent (3.55 g).

For the synthesis of 3STH004, 2STH187 underwent a displacement of the tosylate with sodium azide (Scheme 7).

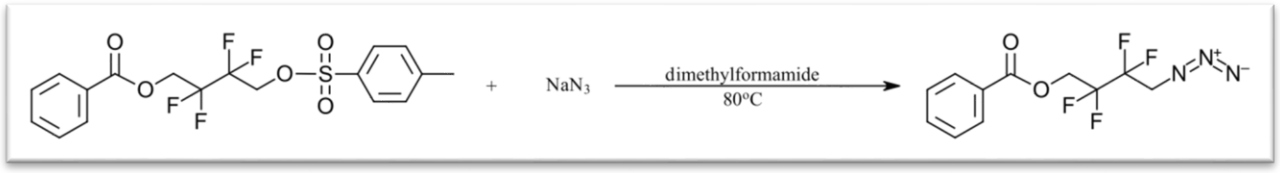

Scheme 7. *Organic azide synthesis. (Created by Joshua Kim)*

4-azido-2,2,3,3-tetrafluorobutyl benzenecarboxylate (Epifanov et al., 2021). 2STH187 was dissolved in dimethyl formamide (25 mL), followed by 1.08 grams of sodium azide. Solution was heated to 80 degrees Celsius and refluxed using a condenser. After reaction ran overnight, deionized water (20 mL) and diethyl ether (20 mL) were introduced to mixture. Reaction was

extracted 2 times with diethyl ether, then washed 3 times with deionized water and 1 time with sodium chloride (40 mL). After a drying step with magnesium sulfate, 3STH004 was isolated *in vacuo* for a yield of 57.8 percent (1.39 g).

A model 3+2 cycloaddition of 3STH004 was also completed (Scheme 8).

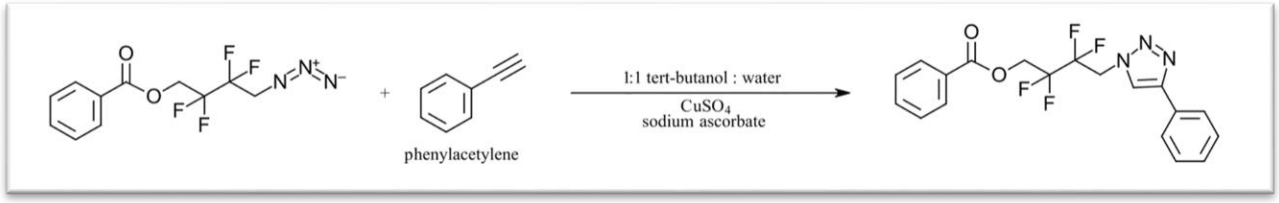

Scheme 8. *Model Monomer **4** Synthesis. (Created by Joshua Kim)*

2,2,3,3-tetrafluoro-4-(4-phenyl-1H-1,2,3-triazol-1-yl)butyl benzenecarboxylate (Jia & Zhu, 2010). 3STH004 (0.46 g) was poured into a solution of phenylacetylene (0.133 g), copper sulfate (2 mL), sodium ascorbate (200 μL), and tert-butanol/water (1:1), which was stirred at room temperature (Scheme 8). After it had run overnight, reaction was extracted 3 times with ethyl acetate (15 mL). Organic layer was washed 1 time with deionized water (15 mL) and 1 time with sodium chloride (10 mL), then dried with magnesium sulfate. Remaining solution was filtered, and product was concentrated *in vacuo* for a yield of 81.3 percent (0.401 g).

QCM Analysis

Prior to performing an analysis of the polymers previously made by Hobson Research Group, a baseline test was performed on the QCM using crystals coated with PEVA, the polymer with which the MIPs blend to adhere to the quartz crystal. This procedure served to establish a protocol for the QCM as well as to examine its accuracy and precision. Onto a 10 MHz quartz crystal was drop-coated 25 μL of PEVA (0.5wt% in toluene). The thin film was allowed to dry overnight. The chemical of choice for this test was chloroform, due to its high affinity for PEVA.

Procedures were gathered from a previous study (Schneider et al., 1998). Three solutions of chloroform were prepared with water as the diluent. Testing began by pumping deionized water from a syringe into the QCM cell for 2 minutes at a flow rate of 2 ml/min. Once a stable frequency was established, the diluted chloroform solutions were then added in a stepwise manner, starting with the lowest concentration of chloroform (0.075% by weight) and increasing from there (0.15% and 0.60% by weight). Each solution was added at a rate of 2 mL/min for a total of 2 minutes. The water temperature remained constant to minimize any changes to liquid density.

After establishing a protocol with the QCM, an MIP imprinted with octanoic acid (STH153) was tested for binding against individual solutions of octanoic acid (OA), PFOA, and acetic acid (AA) at 0.05wt%. Onto a 10 MHz crystal was drop-coated 50 μL of PEVA/STH153 (90:10) 0.05wt% in toluene. The coat was allowed to dry overnight. Testing began by pumping deionized water into the QCM cell via a syringe pump for 3 minutes at a flow rate of 2 mL/min. The diluted solutions were then added individually for 2 minutes at a rate of 2 mL/min. After the pass of each analyte solution, an intervening buffer of deionized water was pumped at 2 mL/min for 3 minutes for the purpose of returning to baseline frequency. The water temperature remained constant to minimize any changes to liquid density.

Results

Two monomer syntheses were conducted, and their identity was verified using IR spectroscopy and column chromatography. Nonfluorinated monomer **3** was synthesized in a 3-step reaction (Scheme 4), and, prior to column chromatography, had a percent yield of 74.4; however, thin-layer chromatography (TLC) results display strong similarity to starting reagent (4-azidobutyl benzoate), indicating probable presence of reactant. To purify **3**, column

chromatography was performed. Possessing a structure of higher polarity, 4-azidobutyl benzoate eluted first. Later fractions, indicated by TLC to be product, were recombined. Concentration of recombined fractions *in vacuo* yielded no evidence of the presence of **3**.

Fluorinated model compound 4 was synthesized in a 4-step reaction (Schemes 5-8). Analysis via TLC indicates that 3STH004 is distinct and isolated from starting reagent. With separation from reactant established, 3STH004 underwent a reaction to form **4**. The workup of this model compound is currently underway to achieve isolation from 3STH004.

During the creation of QCM protocol, the PEVA-coated crystal yielded a significant decrease in resonance frequency compared to the uncoated crystal (Figures 7, 8).

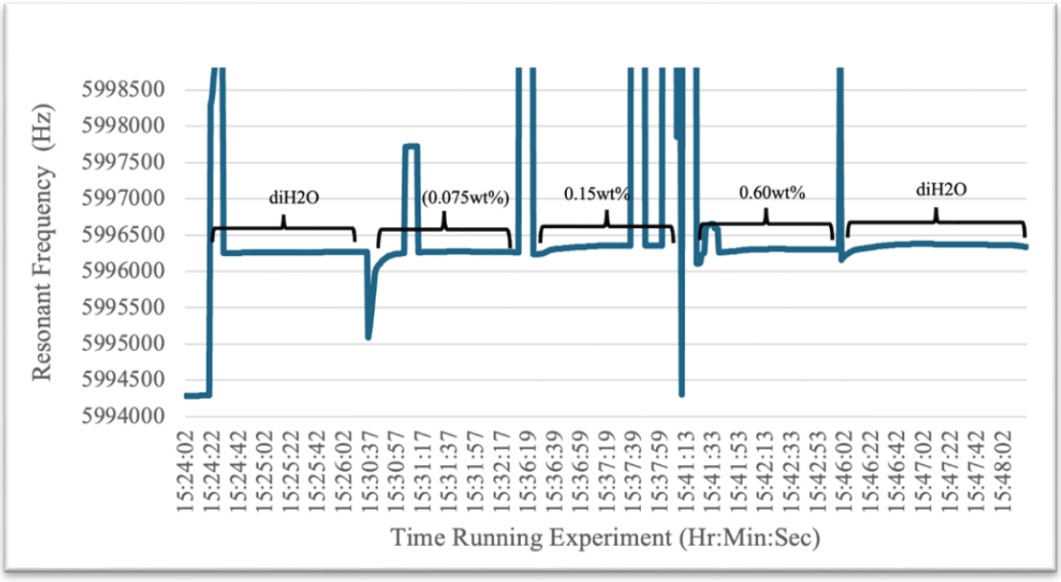

Figure 7. *QCM Data of Uncoated Crystal.*

Note. The following five rounds were pumped through the QCM cell: deionized water, chloroform/water (0.075wt%), chloroform/water (0.15wt%), chloroform/water (0.60wt%), and deionized water. Only time spent running experiment is included, with the idle time between

rounds excised. Drop in resonant frequency between solutions is due to removal of quartz crystal for drying to prevent formation of bubbles in QCM cell.

Figure 8. *QCM Data of PEVA-Coated Crystal.*

Note. The following five rounds were pumped through the QCM cell: deionized water, chloroform/water (0.075wt%), chloroform/water (0.15wt%), chloroform/water (0.60wt%), and deionized water. Only time spent running experiment is included, with the idle time between rounds excised. Drop in resonant frequency between solutions is due to removal of quartz crystal for drying to prevent formation of bubbles in QCM cell.

The change in frequency remained relatively constant for each solution, indicating the establishment of equilibrium in the PEVA-chloroform interaction. The 0.15wt% dilution of chloroform, however, had a sharp peak at the start of the flow. Overall, the resonant frequency slowly decreased from deionized water to 0.15wt%, before it increased for the solution of 0.60wt%.

The analysis of STH153 via QCM gave way to numerous positive changes in resonance in response to the analyte solutions (Figure 9).

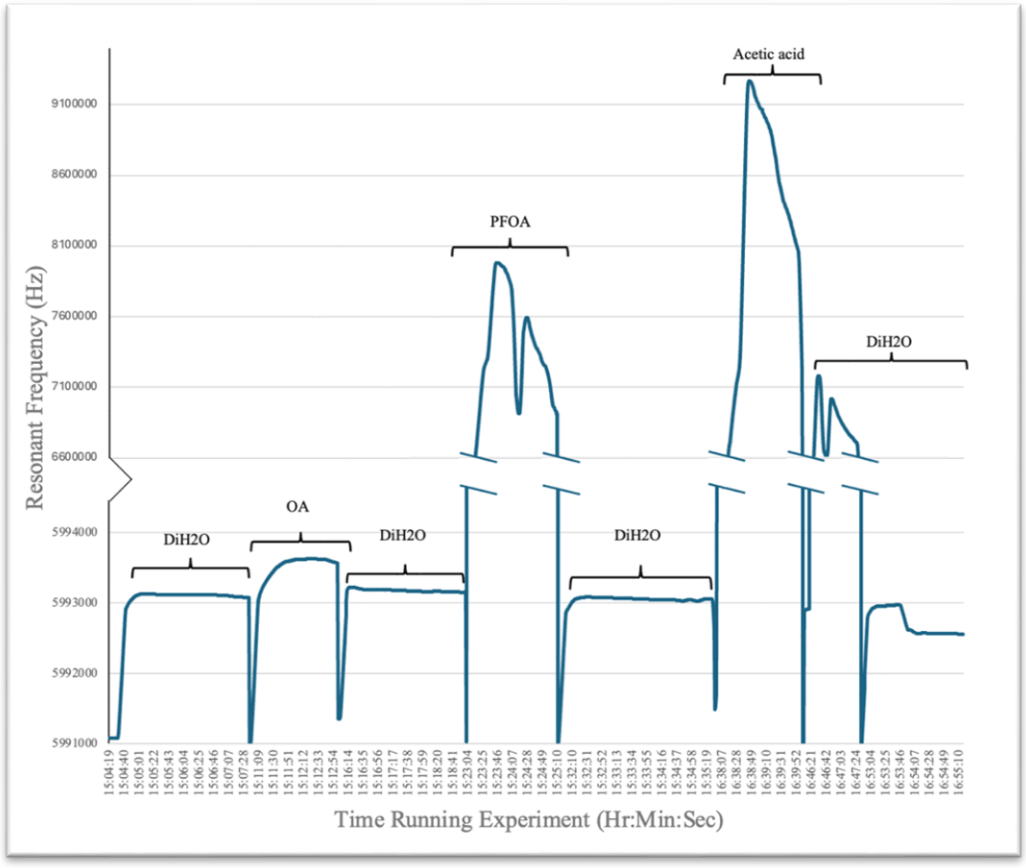

Figure 9. *Raw QCM Data of MIP/PEVA-Coated Crystal.*

Note. The following 3 solutions were pumped through QCM cell: AA, OA, and PFOA at 0.05wt%. Analyte solution flow was interspersed with deionized water flow. Y axis is split to prevent skewing of data.

For the deionized water and OA solutions, the resonant frequency remained stable; however, during the flow of PFOA and AA, the frequency failed to stabilize and had a sharp ascent and descent. After each pass of deionized water, the resonant frequency appeared to return to baseline.

Discussion

Monomer Syntheses

The monomer syntheses produced mixed results. Nonfluorinated **3** was unable to be synthesized, with the third reaction in the synthesis failing to yield any monomer. One factor that may have contributed to this unexpected result was a contaminated mobile phase in the column chromatography caused by impurities in the ethyl acetate solvent. The separation of fluorinated **4** has yet to be performed. However, if **4** is successfully isolated, the optimized conditions of the model reaction will be used by the Hobson group to synthesize a perfluoro monomer.

QCM Protocol

When performing QCM analysis, a decrease in resonance signifies an increase in mass caused by analyte binding. Thus, the QCM protocol was deemed a success, as the PEVA-coated crystal demonstrated a general decrease in resonant frequency upon contact with chloroform solutions, while the frequency of the uncoated crystal remained relatively unchanged (Figures 7, 8). Another strength of the protocol involved the stability of the peaks of the coated crystal, which remained steady during the flow of each solution (Figure 8). The sharp peak of frequency for the 0.15wt% dilution is likely a result of the increase in pressure caused by the entry of water entering the cell. Regarding the 0.6wt% dilution, a response of decreased resonant frequency was expected, and it is unknown why the resonance was elevated. Serving to flush out remaining chloroform molecules in the cell, the final two minutes of deionized water failed to return the frequency of the crystal to baseline. This response, though, is assumed to be due to lack of flow time, as the original study from which the protocol was borrowed performed a 15-minute flush of deionized water to remove residual chloroform (Schneider et al., 1998).

QCM MIP Analysis

The analysis of the MIP included three analyte solutions: acetic acid, octanoic acid, and PFOA. As the MIP was encoded for octanoic acid, it was hypothesized to bind to octanoic acid and PFOA preferentially, due to their similarity in size and shape. Acetic acid served as a control to verify whether binding was driven by structure and size or by the hydrogen bond donor of carboxylic acid present on all three molecules. Similarly to the chloroform protocol analysis, the MIP analysis was expected to have steady peaks that reached an equilibrium during flow of solution.

The raw QCM data possessed a positive change in frequency, an unexpected result that stood in contrast to the negative frequency change of the chloroform protocol test (Figures 7-9). The cause behind this deviation from the expected data is unknown, but it was postulated that the 0.05wt% analyte solutions were too concentrated. As a result, the Sauerbrey equation was not applied to the acquired raw data. In order to generate data that verifies the results of Seacoast Science, the analyte solutions likely need to be diluted 100-fold or 1000-fold.

Conclusions

To conclude, the unpublished previous work of this project was reviewed, a crosslinking fluorinated monomer was synthesized, and QCM analysis was performed. The production of a protocol for testing MIP binding was established and then employed in the analysis of STH153, a nonfluorinated polymer. QCM analysis of STH153 produced peculiar positive peaks, indicating that the concentration of the analyte solutions was likely too high and distorted the frequency. Concerning syntheses, a fluorinated polymer was not produced in this study but remains the most promising method for extracting PFAS. The results of this study add to the expanding field of

fMIPs as well as contribute to the eventual detection and removal of these toxic compounds from water resources.

Future Work

In the future, this study aims to synthesize functionalized crosslinking monomers using the 3+2 cycloaddition demonstrated by **3** and **4** (Schemes 4-8). If purified and isolated in high yields, these monomers will undergo polymerization in the presence of octanoic acid, PFOA, PFOS, and without a template molecule. Analysis of polymer binding affinity and selectivity will be performed via QCM. Binding efficiency will be determined by QCM results and the incorporation of the Sauerbrey equation (Equation 1), which will adjust for polymer mass on MIP-coated QCM chips. Additionally, STH153 will be reexamined for adsorption in the QCM to confirm Seacoast Science data using solutions of OA, AA, and PFOA at higher dilutions.

References

Andersson, L., Sellergren, B., & Mosbach, K. (1984). Imprinting of amino acid derivatives in macroporous polymers. *Tetrahedron Letters, 25*(45), 5211-5214.

Bates, R. W., & Dewey, M. R. (2009). A formal synthesis of swainsonine by gold-catalyzed allene cyclization . *Organic Letters, 11*(16), 3706-3708. https://pubs.acs.org/doi/10.1021/ol901094h

BelBruno, J. J. (2019). Molecularly imprinted polymers. *Chemical Reviews, 119*(1), 94-119. https://10.1021/acs.chemrev.8b00171

Cennamo, N., D'Agostino, G., Porto, G., Biasiolo, A., Perri, C., Arcadio, F., & Zeni, L. (2018). A molecularly imprinted polymer on a plasmonic plastic optical fiber to detect perfluorinated compounds in water. *Sensors (Basel, Switzerland), 18*(6), 1836. https://10.3390/s18061836

Coperchini, F., Awwad, O., Rotondi, M., Santini, F., Imbriani, M., & Chiovato, L. (2017). Thyroid disruption by perfluorooctane sulfonate (PFOS) and perfluorooctanoate (PFOA). *Journal of Endocrinological Investigation, 40*(2), 105-121. https://10.1007/s40618-016-0572-z

Dewey, M. R. (2010). *Synthesis of heterocycles using metal and base catalysis* (Doctoral dissertation). [Doctoral dissertation, Nanyang Technological University, Singapore]. Digital Repository of NTU. https://dr.ntu.edu.sg/handle/10356/47502

Effting, L. M., Urbano, A., do Lago, A. C., de Figueiredo, E. C., & Tarley, C. R. T. (2024). Synthesis of novel oxytetracycline-molecularly imprinted polymer using a semi-covalent chemical imprinting approach for magnetic dispersive solid phase extraction of tetracyclines in water and milk samples. *Food Chemistry, 437,* 137854. https://10.1016/j.foodchem.2023.137854

Epifanov, M., Mo, J. Y., Dubois, R., Yu, H., & Sammis, G. M. (2021). One-pot deoxygenation and substitution of alcohols mediated by sulfuryl fluoride. *Journal of Organic Chemistry, 86*(5), 3768-3777. https://pubs.acs.org/doi/10.1021/acs.joc.0c02557

Espartero, L. J. L., Yamada, M., Ford, J., Owens, G., Prow, T., & Juhasz, A. (2022). Health-related toxicity of emerging per- and polyfluoroalkyl substances: Comparison to legacy PFOS and PFOA. *Environmental Research, 212*(Pt C), 113431. https://10.1016/j.envres.2022.113431

Fei, C., McLaughlin, J. K., Lipworth, L., & Olsen, J. (2009). Maternal levels of perfluorinated chemicals and subfecundity. *Human Reproduction (Oxford, England), 24*(5), 1200-1205. https://10.1093/humrep/den490

Hua, Y., Ahmadi, Y., & Kim, K. (2022). Molecularly imprinted polymers for sensing gaseous volatile organic compounds: Opportunities and challenges. *Environmental Pollution, 311,* 119931. https://10.1016/j.envpol.2022.119931

Huang, J., Wei, Z., & Chen, J. (2008). Molecular imprinted polypyrrole nanowires for chiral amino acid recognition. *Sensors and Actuators B: Chemical, 134*(2), 573-578. https://10.1016/j.snb.2008.05.038

Huang, X., Bai, Q., Hu, J., & Hou, D. (2017). A practical model of quartz crystal microbalance in actual applications. *Sensors (Basel, Switzerland), 17*(8)https://10.3390/s17081785.

Jia, Z., Wen, H., Huang, S., Luo, Y., Gao, J., Wan, R., Wan, K., & Xue, W. (2022). “Click” assembly of novel dual inhibitors of AChE and MAO-B from pyridoxine derivatives for the treatment of Alzheimer’s disease. *Heterocyclic Communications, 28*(1), 18-25. https://doi.org/10.1515/hc-2022-0002

Jia, Z., & Zhu, Q. (2010). ‘Click’ assembly of selective inhibitors for MAO-A. *Bioorganic & Medicinal Chemistry Letters, 20*(21), 6222-6225. https://10.1016/j.bmcl.2010.08.104

Joensen, U. N., Bossi, R., Leffers, H., Jensen, A. A., Skakkebæk, N. E., & Jørgensen, N. (2009). Do perfluoroalkyl compounds impair human semen quality? *Environmental Health Perspectives, 117*(6), 923-927. https://10.1289/ehp.0800517

Kamendulis, L. M., Hocevar, J. M., Stephens, M., Sandusky, G. E., & Hocevar, B. A. (2022). Exposure to perfluorooctanoic acid leads to promotion of pancreatic cancer . *Carcinogenesis, 4*(43), 469-478. https://pubmed.ncbi.nlm.nih.gov/35022659/

Kim, Joshua (member of Hobson Research Group, personal communication, March 5, 2024)

Kirisenage, P. M., Zulqarnain, S. M., Myers, J. L., Fahlman, B. D., Mueller, A., & Marquez, I. (2022). Development of adsorptive membranes for selective removal of contaminants in water. *Polymers, 14*(15), 3146. https://10.3390/polym14153146

Kong, Z., Lu, L., Zhu, C., Xu, J., Fang, Q., Liu, R., & Shen, Y. (2022). Enhanced adsorption and photocatalytic removal of PFOA from water by F-functionalized MOF with in-situ-growth TiO2: Regulation of electron density and bandgap. *Separation and Purification Technology, 297*, 121449. https://10.1016/j.seppur.2022.121449

Li, L., Tang, W., & Zhao, Z. (2009). Synthesis and application of phenyl-derived photo affinity probes. *Chinese Journal of Chemistry, 27*(7), 1391-1396. https://onlinelibrary.wiley.com/doi/abs/10.1002/cjoc.200990233

Liang, L., Pan, Y., Bin, L., Liu, Y., Huang, W., Li, R., & Lai, K. P. (2022). Immunotoxicity mechanisms of perfluorinated compounds PFOA and PFOS. *Chemosphere, 291*(Pt 2), 132892. https://10.1016/j.chemosphere.2021.132892

Lübke, M., Whitcombe, M. J., & Vulfson, E. N. (1998). A novel approach to the molecular imprinting of polychlorinated aromatic compounds. *Journal of the American Chemical Society, 120*(51), 13342-13348. https://10.1021/ja9818295

Nortcliffe, A., Ekstrom, A. G., Black, J. R., Ross, J. A., Habib, F. K., Botting, N. P., & O'Hagan, D. (2014). Synthesis and biological evaluation of nitric oxide-donating analogues of sulindac for prostate cancer treatment. *Bioorganic & Medicinal Chemistry, 22*(2), 756-761. https://10.1016/j.bmc.2013.12.014

Pan, M., Li, R., Xu, L., Yang, J., Cui, X., & Wang, S. (2018). Reproducible molecularly imprinted piezoelectric sensor for accurate and sensitive detection of ractopamine in swine and feed products. *Multidisciplinary Digital Publishing Institute, 18*(6) https://www.mdpi.com/1424-8220/18/6/1870

Patil, V. M., & Masand, N. (2018). Chapter 12 – anticancer potential of flavonoids: Chemistry, biological activities, and future perspectives. *Studies in Natural Products Chemistry, 59*, 401-430. https://10.1016/B978-0-444-64179-3.00012-8

Schneider, T. W., Frye-Mason, G. C., Martin, S. J., Spates, J. J., Bohuszewicz, T. V., Osbourn, G. C., & Bartholomew, J. W. (1998). Chemically selective coated quartz crystal microbalance (QCM) array for detection of volatile organic chemicals. *Chemical Microsensors and Applications, ,* 85-94. https://www.osti.gov/biblio/1541

Sibrian-Vazquez, M., & Spivak, D. A. (2004). Molecular imprinting made easy. *Journal of the American Chemical Society, 126*(25), 7827-7833. https://datapdf.com/molecular-imprinting-made-easy-journal-of-the-american-chemi3ce7d9a8a63059bfa1914e1b711868e785281.html

Steenland, K., Hofmann, J. N., Silverman, D. T., & Bartell, S. M. (2022). Risk assessment for PFOA and kidney cancer based on a pooled analysis of two studies. *Environment International, 167*(107425) https://doi.org/10.1016/j.envint.2022.107425

Tamayo, F. G., Turiel, E., & Martín-Esteban, A. (2007). Molecularly imprinted polymers for solid-phase extraction and solid-phase microextraction: Recent developments and future trends - ScienceDirect. *Journal of Chromatography A, 1152*(1-2), 32-40. https://www.sciencedirect.com/science/article/pii/S0021967306016864

Tan, X., Sawczyk, M., Chang, Y., Wang, Y., Usman, A., Fu, C., Král, P., Peng, h., Zhang, C., & Whittaker, A. K. (2022). Revealing the molecular-level interactions between cationic fluorinated polymer sorbents and the major PFAS pollutant PFOA . *Macromolecules, 55*(3), 1077-187. https://10.1021/acs.macromol.1c02435

Teaf, C. M., Garber, M. M., Covert, D. J., & Tuovila, B. J. (2019). Perfluorooctanoic acid (PFOA): Environmental sources, chemistry, toxicology, and potential risks. *Soil and Sediment Contamination: An International Journal, 28*(3), 258-273. https://10.1080/15320383.2018.1562420

Wang, Y., Wang, L., Li, J., Liang, Y., Ji, H., Zhang, J., Zhou, Q., & Jiang, G. (2014). The mechanism of immunosuppression by perfluorooctanoic acid in BALB/c mice. *Toxicology Research, 3*(3), 205-213. https://10.1039/C3TX50096A

Wang, Y., Wang, L., Liang, Y., Qiu, W., Zhang, J., Zhou, Q., & Jiang, G. (2011). Modulation of dietary fat on the toxicological effects in thymus and spleen in BALB/c mice exposed to perfluorooctane sulfonate. *Toxicology Letters, 204*(2-3), 174-182. https://10.1016/j.toxlet.2011.04.029

Wee, S. Y., & Aris, A. Z. (2023). Revisiting the “forever chemicals”, PFOA and PFOS exposure in drinking water. *Nature Portfolio Journals, 6*(57) https://doi.org/10.1038/s41545-023-00274-6

Zhang, L., Yu, H., Chen, H., Huang, Y., Bakunina, I., de Sousa, D. P., Sun, M., & Zhang, J. (2023). Application of molecular imprinting polymers in separation of active compounds from plants. *Fitoterapia, 164*, 105383. https://10.1016/j.fitote.2022.105383

Zheng, X., Lian, Q., Yang, H., & Wang, X. (2016). Surface molecularly imprinted polymer of chitosan grafted poly(methyl methacrylate) for 5-fluorouracil and controlled release . *Scientific Reports, 6*(21409)https://https://doi.org/10.1038/srep21409

Zhong, Y., Shen, L., Ye, X., Zhou, D., He, Y., & Zhang, H. (2020). Mechanism of immunosuppression in zebrafish (danio rerio) spleen induced by environmentally relevant concentrations of perfluorooctanoic acid. *Chemosphere, 249*, 126200. https://10.1016/j.chemosphere.2020.126200

Zu, B., Pan, G., Guo, X., Zhang, Y., & Zhang, H. (2009). Preparation of molecularly imprinted polymer microspheres via atom transfer radical precipitation polymerization. *Journal of Polymer Science Part A: Polymer Chemistry, 47*(13), 3257-3270. https://10.1002/pola.23389